Vibrational Coherence in Photosynthetic Reaction Centers Observed in the Bacteriochlorophyll Anion Band

ARTICLE *in* THE JOURNAL OF PHYSICAL CHEMISTRY B · AUGUST 1998

Impact Factor: 3.3 · DOI: 10.1021/jp9817473

3 AUTHORS, INCLUDING:

Josef Wachtveitl
Goethe-Universität Frankfurt am Main
180 PUBLICATIONS **3,710** CITATIONS

Vibrational Coherence in Photosynthetic Reaction Centers Observed in the Bacteriochlorophyll Anion Band

S. Spörlein, W. Zinth, and J. Wachtveitl*

Institut für Medizinische Optik, Ludwig-Maximilians-Universität, Oettingenstrasse 67, 80538 München, Germany

Received: April 3, 1998; In Final Form: July 1, 1998

Oscillatory components of the absorption changes in reaction centers from *Rhodobacter sphaeroides* are observed by femtosecond spectroscopy in the spectral region between 920 and 1100 nm covering the ranges of excited-state absorption and stimulated emission of the photoexcited primary donor and the long wavelength absorption band of the bacteriochlorophyll anion. These oscillations with a dominant frequency of 135 cm^{-1} are damped on the 0.4−0.8 ps time scale. The observations fit well into a model with vibrational wave packet motion on the excited-state potential surface modulating stimulated emission. Amplitudes and phases of the oscillation do not show any peculiarity within the absorption band of the bacteriochlorophyll anion, indicating that the interaction of this wave packet with electron transfer to the accessory bacteriochlorophyll is not required to explain the experimental data.

Introduction

Oscillatory features with frequencies in the 100 cm^{-1} regime have been observed in a number of transient absorption experiments of the primary electron transfer of photosynthetic reaction centers (RC).[1−4] The first observation[1] in 1991 triggered a series of other experiments and discussions on the biological relevance of these modulations and on the importance for the photosynthetic electron transfer.[2] Detailed experiments have shown that the observed modulations originate from the motion of a vibrational wave packet on the S_1 potential energy surface of the primary donor, the special pair P.[2] In the analysis of the data typical vibrational frequencies up to 230 cm^{-1} have appeared. Since similar frequencies were deduced from the temperature dependence of the primary electron transfer for the vibrational modes coupled to the primary electron-transfer process,[5−7] a close connection of the S_1 wave packet motion and electron transfer was suggested but could not be proven. This was not surprising considering the well-known properties of primary electron transfer: if the first electron-transfer step away from P* occurs with $\tau \cong 3$ ps and the decay of the stimulated emission with 3 ps — strongly supports this interpretation[8,9] — a wave packet like excitation of vibrational modes above 100 cm^{-1} coupled to electron transfer should cause only weak modulations of the populations (see e.g. Figure 5a−c). In addition, until now modulated absorption transients were published only at wavelengths with a dominating stimulated emission signal or in congested spectral regions.[1−4] As a consequence, it was not possible so far to distinguish between contributions from modulated excited-state absorption and those from modulated population of product states.

In this paper we present results from experiments with femtosecond time resolution performed in the spectral range between 920 and 1100 nm. While in the short wavelength range the absorption transients are dominated by stimulated emission from P* (920−990 nm), the signal decreases strongly toward longer wavelengths. The strong contribution from $P^+B_A^-$ around 1020 nm originating from a pronounced bacteriochlorophyll anion band[10−12] should allow the optimum detection of a modulated formation of $P^+B_A^-$ at this wavelength with only small interference from other intermediates.

Materials and Methods

Sample Preparation. The reaction centers of *Rb. sphaeroides* strain R26.1 were prepared according to the procedure described elsewhere.[13] Since the same sample was used for experiments at cryogenic temperatures, it contained 55% (v/v) glycerol. To avoid an accumulation of long-lived photoproducts, 50 mM dithiothreitol was added to prereduce the quinone electron acceptor Q_A. For this reason the rates of the primary reactions are somewhat slower than in the unreduced samples. The concentration of the 1 mm sample was adjusted to a transmission of 10% at 865 nm at room temperature.

Time-Resolved Experiments. The transient absorption changes were recorded in a femtosecond pump−probe setup as described in detail elsewhere.[14] Briefly, light pulses for the measurements are generated by a Ti:sapphire laser system operating at a wavelength of 870 nm with a pulse duration of 60 fs. Subsequently, the energy was increased by a regenerative amplifier (repetition rate 20 Hz), and a small fraction of this energy was used in the experiment. The 100 fs pulse was split into two parts: one part (0.14 μJ) was used for the excitation after passing through a cell with a saturable absorber (IR143, Lambda Physik, Germany); the other part (1−2 μJ) was focused into a 2 mm sapphire crystal to generate a white light continuum. This pulse was recompressed in a grating setup that also was used to select the appropriate wavelength band, providing tunable probing pulses. The detection system has been described previously.[15] It was optimized to resolve absorbance changes smaller than 0.1% with a high temporal resolution. The temporal instrumental response function was determined for each measurement in an independent experiment by recording two-photon absorption in a glass filter (Schott, RG780). The filter (thickness of 1 mm) was covered with 1 mm cuvette windows

* Corresponding author. Phone +49 89 2178-2937. Fax +49 89 2178-2902. E-mail Josef.Wachtveitl@physik.uni-muenchen.de.

S1089-5647(98)01747-7 CCC: $15.00
Published on Web 08/27/1998

in order to simulate the conditions of the pump and probe experiment in the sample cell. Throughout the entire spectral range investigated in this paper the width (fwhm) of the cross-correlation function was less than 110 fs. The polarizations of the pump and probe pulses were parallel to each other.

The time-resolved measurements in the gain region were performed up to long delay times ($t_d = 1$ ns) to allow a reliable determination of the P* decay constants. The time axes in the figures are restricted to the 1 ps range for optimal visualization of the early oscillatory components.

Modeling of the Transient Absorption Changes. The ultrafast absorption dynamics observed in the RC contain a number of contributions. Therefore, a special procedure is required to obtain a clear separation of the part related to wave packet like processes. The elaboration follows the lines suggested by the theory of ET processes: at later times nonadiabatic ET theory applies, and the processes can be described by exponential functions. In the data analysis the exponentials are convoluted with the instrumental response function which is approximated by a Gaussian. At early times adiabatic processes or wave packet motions could appear. The experimental consequence is nonexponential behavior such as oscillatory contributions. One prominent feature of wave packet motion is the first part of the oscillation period on the S_1 potential surface which leads to a delayed start of the red wing of stimulated emission and causes a strong signal change at early delay times. For the modeling of the experimental data we proceed as follows: (i) Time constants for the exponential model function and a first estimate for the amplitudes are deduced from absorption changes recorded at later delay times. (ii) A qualitative averaging over most parts of the oscillations was obtained by using the exponential model functions in combination with the measured time zeros, but considering a delayed rise of stimulated emission (solid curves in Figure 1). (iii) Using the amplitudes and decay times determined in (ii), while neglecting the delayed rise of stimulated emission, we calculated curves that should contain the total contributions related to an exponential behavior of the RC (broken curves in Figure 1). (iv) The difference between the broken curve and the experimental data should approximate the nonexponential contribution. This residual signal was normalized to the amplitude of the (delayed) stimulated emission (curves in Figure 3).

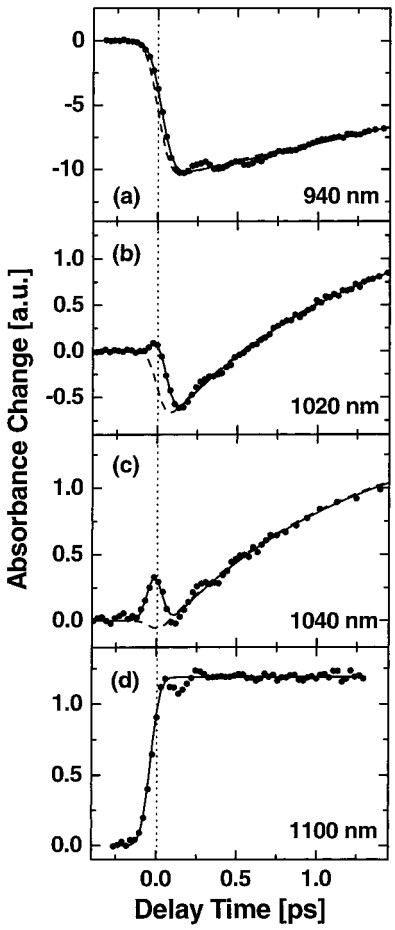

Figure 1. Transient absorbance changes of wild-type RCs (R26.1) at four selected probing wavelengths (solid circles). The best approximation of the data using the fitting procedure described in the Materials and Methods section is drawn as a solid line. Here, the delayed onset of the stimulated emission signal of P* is considered. The dashed lines represent the best curves obtained, when setting the delay between the instananeous (excited-state-absorption) and delayed (stimulated emission) component of P* to zero. These curves are used for calculating the residuals shown in Figure 3 by subtracting the dashed line from the original data.

Results

Figure 1 shows a set of transient absorption data taken throughout the investigated spectral range. At a probing wavelength of $\lambda_{pr} = 940$ nm on the red side of the peak of the stimulated emission (Figure 1a), we observe a rapid decrease of the signal briefly after time zero, caused by the onset of the stimulated emission. Later on, an absorption rise reflects the decay of the P* population. The detailed modeling shows that the initial transient is slightly delayed by ≅40 fs and that modulations appear during the first picosecond.

Close to the peak of the anion band of the bacteriochlorophyll at $\lambda_{pr} = 1020$ nm (Figure 1b) the signal behavior is more complex: at time zero a weak absorption increase points to the instantaneous start of excited-state absorption; the subsequent absorption decrease can be related to the delayed appearance of stimulated emission, which is weak at this wavelength. The following absorption rise with $\tau_2 \cong 1.3$ ps is related to the developing B_A^- population. The effect of the modulation is still visible; however, it is less pronounced than at 940 nm. At $\lambda_{pr} = 1040$ nm (Figure 1c) in the red wing of the B_A^- band similar absorption features appear. However, excited-state absorption becomes more important while stimulated emission and B_A^- absorption lose importance. At a very long probing wavelength of $\lambda_{pr} = 1100$ nm (Figure 1d), the signal is dominated by excited-state absorption and induced absorption from P^+ with approximately the same amplitude. A remaining modulation with one period at early delay times indicates that weak stimulated emission may occur briefly after excitation.

The fit of the exponential functions to the transient absorption changes yields time constants of $\tau_1 = 3.3$ ps (P* decay) and $\tau_2 = 1.3$ ps (depopulation of $P^+B_A^-$). The latter time constant is somewhat longer than the 0.9 ps time found in RC with unreduced quinones.[11,16] This increase in reaction time is presumably due to electrostatic repulsion from the negative charge at the quinone Q_A.

The amplitudes of the exponentials deduced from the modeling procedure can be used to calculate the difference cross-section spectra of the intermediates when a stepwise ET reaction model is used (see Figure 2). The observation of a delayed rise of stimulated emission combined with instantaneous excited-state absorption allows the separation of these two contributions for $\lambda_{pr} > 920$ nm. The absorption cross sections determined in this way follow the results obtained previously:[11] while stimu-

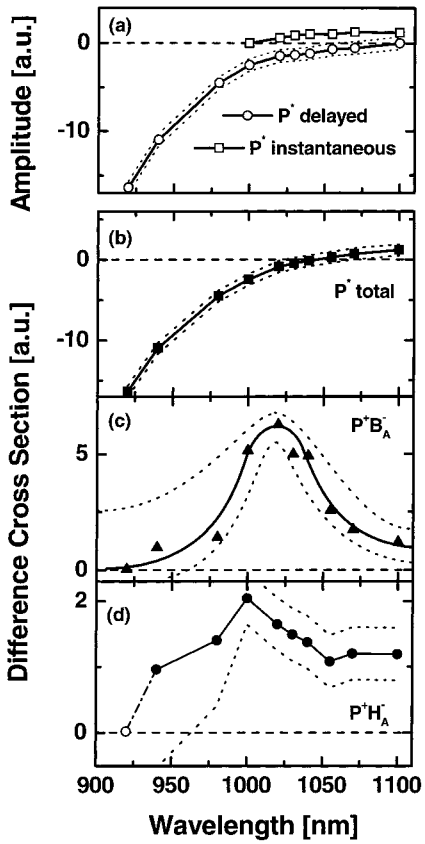

Figure 2. (a) Amplitude spectrum of the two P* contributions: the instantaneous excited-state absorption (open squares) and the delayed stimulated emission (open circles; broken line: error range). In the wavelength range <1020 nm a precise determination of the amplitude of the excited-state absorption is not possible because of the large amplitude of the stimulated emission. (b−d) Difference cross sections of intermediate states: the solid squares represent the difference cross section of P* calculated from the sum of the contributing P* amplitudes, and the solid triangles represent the $P^+B_A^-$ difference cross section. The wavelength dependence of the $P^+H_A^-$ absorption (solid circles) is identical to the absorption of P^+ because the pheophytin anion H_A^- does not absorb in this wavelength range. The larger errors at shorter wavelengths result from the small investigated time range.

lated emission is strong at 940 nm and continuously decreases with increasing wavelength, excited-state absorption becomes more important at $\lambda_{pr} > 1020$ nm. The strong absorption band around 1020 nm in the bacteriochlorophyll anion region represents the formation of the intermediate $P^+B_A^-$. At later times the signal is dominated by the cation radical P^+, which is present in both states $P^+B_A^-$ and $P^+H_A^-$. The bacteriopheophytin anion radical H_A^- does not contribute in the investigated spectral range.[10]

The oscillatory deviations of the measured data points from the exponential fit functions are summarized in Figure 3. They are normalized to the amplitude of the stimulated emission. All curves show a strong positive peak at zero delay time ($t_D = 0$ fs). Later on, the signal evolves to a first minimum at $t_D \cong 150$ fs and to a secondary peak at $t_D = 300$ fs. In the same curves a subsequent minimum around $t_D = 400-450$ fs is found. The damping of the oscillations occurs in the 0.4−0.8 ps range. The analysis of the data using fast Fourier transform indicates that the main oscillation frequency at all wavelengths $\lambda_{pr} > 920$ nm is around 135 cm^{-1}. For $\lambda_{pr} < 1030$ nm a weaker component around 40 cm^{-1} is observed. Figure 3 clearly shows that frequencies and phases of the high-frequency oscillation persist throughout the whole spectral range and that no apparent peculiarities appear in the bacteriochlorophyll anion absorption

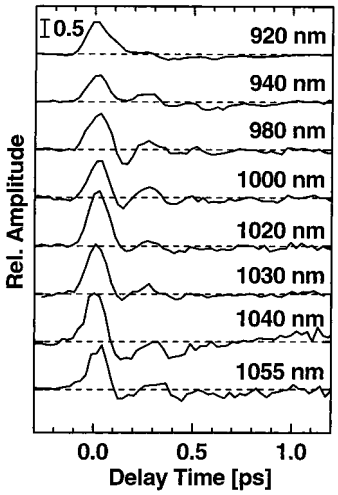

Figure 3. Residuals obtained by subtracting the zero delay fit (dashed curves in Figure 1) from the experimental data (see Figure 1 and text). To allow a better comparison, the plotted graphs are normalized to the amplitude of stimulated emission.

range. However, the modulations seem to be somewhat weaker at 1020 and 1030 nm. The wavelength independence of the amplitudes normalized to the amplitude of the stimulated emission clearly supports a close connection of the oscillations and the stimulated emission process.

Discussion

Excited-State Wave Packet Motion and Its Effect on Transient Absorption. Modulated absorption changes have been observed in very early experiments performed with ultrashort light pulses in the $10^{-14}-10^{-13}$ s regime.[19−22] These modulations could be assigned to the motion of vibrational wave packets. In Figure 4a, this explanation is summarized: excitation by an ultrashort pulse promotes the system to the Franck−Condon region on the S_1 surface. The short duration of the excitation pulse may lead to a vibrational excitation in the form of a coherent superposition of vibrational levels which can be described as a wave packet. Later on this wave packet evolves on the S_1 surface: it oscillates with the vibrational frequency ω_{vib}. Phase and energy relaxation processes lead to the damping and finally to the disappearance of the wave packet. During the S_1 motion the absorption of the molecule is modulated: stimulated emission in the long wavelength range appears delayed by a fraction of the oscillation period. Absorption is changed, when the wave packet passes through the parts of the S_1 surface where the distance to the ground-state surface equals the photon energy of the probing light. This leads to a modulation of the absorption changes with the frequency ω_{vib} of the vibration or with its second harmonic. The relaxation of vibrational energy during wave packet motion causes a situation where the region of the S_1 surface responsible for the very low-energy photons from stimulated emission is reached only once in a single pass. As a consequence, stimulated emission occurs only once in a single flash at very early times. All these features are well observed in the transient absorption data of the photosynthetic RC: (i) The delayed appearance of stimulated emission is well observed in the experimental data. At low temperatures (30 K) we could even find explicitly an increase of the delay with probing wavelength (data not shown). (ii) In the very red wing of stimulated emission (around $\lambda_{pr} = 1100$ nm) we observe only one modulation period, indicating that the corresponding range of the S_1 surface is reached only once during the first vibrational period and not later on. (iii)

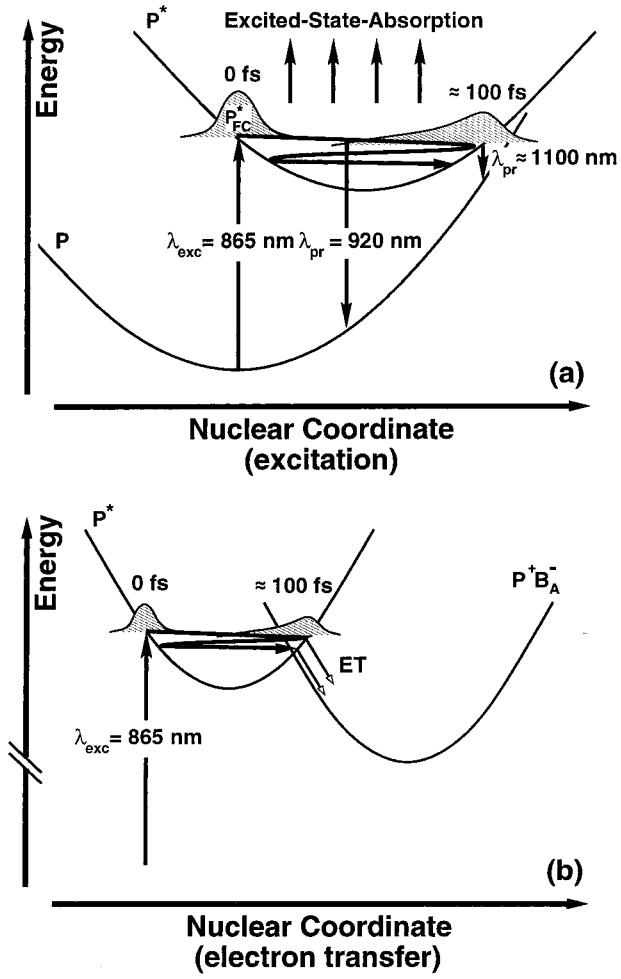

Figure 4. (a) Oscillations due to wave packet motion on a potential energy surface: After excitation (865 nm) from the ground state (P) in the Franck−Condon region of the excited state (P^*_{FC}) the created wave packet moves on the potential energy surface P*. Since excited-state absorption occurs as long as this state is populated, it is detectable instantaneously. After a few tens of femtoseconds the RC has reached the right nuclear configuration to allow observation of stimulated emission. At 1100 nm the signal of stimulated emission is measurable only for a short time of 250 fs (compare Figure 1). At later delay times too much energy was lost by internal energy redistribution, which prevents the system from reaching this nuclear configuration region for a second time. (b) Simplified model for discontinuous electron transfer, based on the calculations described in the text and Figure 5: after excitation the wave packet moves on the potential energy surface of P*. Each time it reaches the intersection region of P* and $P^+B_A^-$ there is a possibility to reach the $P^+B_A^-$ surface. A considerable probability of transfer exists only in a small range of nuclear configurations. Therefore, the P* state will be depopulated stepwise due to the wave packet motion.

Oscillatory features at intermediate wavelengths reflect the oscillation of the wave packet. The frequency analysis of oscillations by Fourier transformation showed main frequencies around 135 cm^{-1} and below (e.g., around 40 cm^{-1} for $\lambda_{pr} <$ 1030 nm). The quickly damped, high-frequency oscillation is described in several investigations,[1−4] and its possible functional importance will be discussed in the next paragraph. From the slow damping of the low-frequency mode observed at 805 nm a possible connection of the 40 cm^{-1} mode to the electron-transfer process was suggested.[4] We find only a weak amplitude of the 40 cm^{-1} oscillation in the B^- range. This does not allow us to draw any conclusions about the role of the 40 cm^{-1} mode in electron transfer. (iv) The instantaneous start of excited-state absorption and its weak modulation (see e.g. at 1100 nm) indicates that excited-state absorption occurs with similar amplitude throughout the whole range of the S_1 potential energy surface that can be probed by the wave packet motion.

Excited-State Wave Packet Motion and Electron Transfer. While the experimental observations can be explained well by the motion of the excited-state wave packet and its action on stimulated emission, we want to discuss here whether the experimental results allow to establish a connection between wave packet motion and electron transfer. In Figure 4b the potential energy surfaces are plotted schematically for standard ET theory where only one relevant vibrational mode is used. Whether this mode is identical to the mode that couples strongly to the optical excitation process (see Figure 4a) cannot be proven. In view of the large number of vibrational modes in the special pair this identity seems unlikely. A modulation of the population of the two states involved, with the frequency of the vibrational motion, can occur as follows: excitation prepares a wave packet on the S_1 potential surface which oscillates back and forth. ET with high efficiency only occurs very close to the intersection of the two potential surfaces with a probability determined by the Landau−Zener factor. For simplicity, we assume in Figure 4 that the potential surfaces cross at the outer turning point of the vibrational motion. Back-reactions from the product state $P^+B_A^-$ are assumed to be irrelevant if fast relaxation or reorganization takes place in $P^+B_A^-$. (Otherwise, a much more complicated behavior would result, and vibrational motion in the product state has to be considered.) The probability of the ET process for each hit of the interaction region should be related to the long time decay of the population of P* (3.3 ps) and the oscillation period (250 fs). From the slow decay of P* and the short oscillation period a probability of $p \cong 0.1$ is calculated, which is close to the value one would assume from a theoretical treatment using the Landau−Zener formalism.[23] In our present approach, we assume such a discontinuous ET for the first reaction from P* to $P^+B_A^-$ and an exponential decay with a time constant of 1.3 ps for the secondary ET step. Within this model, the population of the different states can be estimated (see Figure 5, curves a−d). It should be noted that the details of the reaction model (preparation of the wave packet in the Franck−Condon regime at the inner turning point, reaction at the outer turning point, fast relaxation in $P^+B_A^-$) are designed in order to give optimum modulation of the population densities. In Figure 5 the population densities are multiplied with the absorbance difference cross sections of the respective states at $\lambda = 1020$ nm in order to reproduce the contributions of the different states to the absorption changes at this wavelength for ready comparison with the experimental data. The simplified model used here leads to a stepwise decay of the population of P* with a relative step height of $p \cong 0.1$. However, a stronger modulation occurs for $P^+B_A^-$: (i) Here, the fast depopulation of $P^+B_A^-$ by the secondary ET step leads to a fast reduction of its population (immediately after each formation step). (ii) The fast depopulation (1.3 ps) of $P^+B_A^-$ in combination with a slow formation from P* (3.3 ps) allows only a low peak population of the intermediate state $P^+B_A^-$ of ≈25%. Under these conditions, the relative height of the modulation is strongly increased.

Therefore, the modulation of the population by the vibrational motion should be observable at best in a spectral range with strong contributions from the intermediate state $P^+B_A^-$. From the analysis of the different transient spectra one deduces that the 1020 nm range should be optimal for the detection of $P^+B_A^-$ modulations. Here, $P^+B_A^-$ causes a strong absorption signal, and interference from the wings of the stimulated emission from

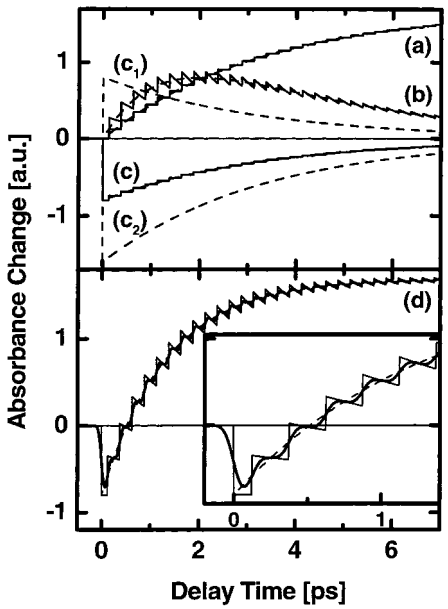

Figure 5. Calculation of the expected transient absorption changes at 1020 nm for the case of a stepwise depopulation of P* and a simultaneous population of $P^+B_A^-$, neglecting the signal contributions arising from modulations of the stimulated emission. Damping of the oscillation is not considered in this calculation. In the upper half the contributions from the three intermediates are plotted, which are detectable at 1020 nm (a, b, c). The solid lines represent the results of the calculations. The dashed lines are drawn for comparison with a model assuming an exponential decay of P*. In detail: absorption ([population] times [difference cross section]) of the P^+ cation (a), the B_A^- anion (b), and P* (c). The latter one is the sum of two parts: the excited-state absorption (c_1) and the stimulated emission (c_2). These two contributions are not distinguished in the model. Their existence is known from measurements described in Figure 2. The expected signal, the sum of the graphs (a−c), is shown in (d). In addition, the convolution of the idealized transient absorbance signal with the instrumental reponse function is depicted as the thick solid line. The following parameters are used for the calculations: cross-correlation width, 110 fs; vibrational period, 250 fs (see text); and mean depopulation time of P*, $\tau_1 = 3.3$ ps, and of $P^+B_A^-$, $\tau_2 = 1.3$ ps. The inset is a magnification showing curve d within the first picosecond.

P* should be weak. Calculated transients for a probing wavelength of 1020 nm are shown in Figure 5 (curve d and insert). Different approaches to the experimental situation are also considered: (i) A temporal δ-function-shaped instrumental response function combined with purely exponential decay processes leads to the kinetics shown as broken curve (standard nonadiabatic theory). (ii) The stepwise formation of $P^+B_A^-$ in combination with a δ-function-shaped instrumental response function results in the curve plotted as the thin solid line. (iii) Combining the stepwise population of $P^+B_A^-$ with the experimentally found instrumental response function yields the thick solid line. The simulation shows that a wave packet like motion of the mode coupling to the ET reaction according to the simplified model given above should be clearly visible under the experimental conditions used, provided that no disturbing effects, e.g., from stimulated emission, are present.

The comparison of the simulation and the experimental data yields no direct indication for a wave packet like modulation of the ET process. Even in the 1020 nm regime the modulation of the weak stimulated emission can still account for the observed signal. This is clear from Figure 3 where this modulation was normalized to the amplitude of the total stimulated emission at the corresponding probing wavelengths. The only peculiarity found is a somewhat weaker modulation in the range of the bacteriochlorophyll anion band. This signal reduction, which is within the experimental precision of the experiment, could be due to a destructive interference between contributions from modulated stimulated emission and the ET process. However the weak amplitudes of the modulations in the original data and the normalization procedure impose considerable uncertainties which do not allow us to make a final decision.

In conclusion, we have shown that modulated absorption features are observed throughout the whole wavelength region of 920−1100 nm. The observed features can be explained well by the motion of a vibrational wave packet on the excited-state potential surface of the special pair P* and its effect on stimulated emission and excited-state absorption. Using a simplified model for an ET process modulated by a wave packet like excitation of the active vibrational mode, we calculated the possible consequences for the experiments in the absorption region of the accessory bacteriochlorophyll anion B_A^-. The analysis shows that to a first-order approximation a modulated ET is not required to explain the observed absorption changes.

Acknowledgment. The authors thank H. Scheer and M. Meyer for the preparation of high-quality R26.1 RC samples.

References and Notes

(1) Vos, M. H.; Lambry, J.-C.; Robles, St. J.; Youvan, D. C.; Breton, J.; Martin, J.-L. *Proc. Natl. Acad. Sci. U.S.A.* **1991,** *88*, 8885.

(2) Vos, M. H.; Rappaport, F.; Lambry, J.-C.; Breton, J.; Martin, J.-L. *Nature* **1993,** *363*, 320.

(3) Vos, M. H.; Jones, M. R.; Hunter, C. N.; Breton, J.; Lambry, J.-C.; Martin, J.-L. *Biochemistry* **1994,** *33*, 6750.

(4) Streltsov, J. M.; Aartsma, T. J.; Hoff, A. J.; Shuvalov, V. A. *Chem. Phys. Lett*. **1997**, *266*, 347.

(5) Fleming, G. R.; Martin, J. L.; Breton, J. *Nature* **1988**, *333*, 190.

(6) Bixon, M.; Jortner, J. *J. Phys. Chem.* **1986**, *90*, 3795.

(7) Kirmaier, C.; Holten, D.; Parson, W. W. *Biochim. Biophys. Acta* **1985**, *810*, 33.

(8) Martin, J. L.; Breton, J.; Hoff, A. J.; Migus, A.; Antonetti, A. *Proc. Natl. Acad. Sci. U.S.A.* **1986**, *83*, 957.

(9) Holzapfel, W.; Finkele, U.; Kaiser, W.; Oesterhelt, D.; Scheer, H.; Stilz, H. U.; Zinth, W. *Proc. Natl. Acad. Sci. U.S.A.* **1990**, *87*, 5168.

(10) Fajer, J.; Brune, D. C.; Davis, M. S.; Forman, A.; Spaulding, L. D. *Proc. Natl. Acad. Sci. U.S.A.* **1975,** *72*, 4956.

(11) Arlt, T.; Schmidt, S.; Kaiser, W.; Lauterwasser, C.; Meyer, M.; Scheer H.; Zinth, W. *Proc. Natl. Acad. Sci. U.S.A.* **1993**, *90*, 11757.

(12) Schmidt, S.; Arlt, T.; Hamm, P.; Huber, H.; Nägele, T.; Wachtveitl, J.; Meyer, M.; Scheer H.; Zinth, W. *Chem. Phys. Lett.* **1994**, *223*, 116.

(13) Holzapfel, W.; Finkele, U.; Kaiser, W.; Oesterhelt, D.; Scheer, H.; Stilz, H. U.; Zinth, W. *Chem. Phys. Lett.* **1989**, *160*, 1.

(14) Huber, H.; Meyer, M.; Nägele, T.; Hartl, I.; Scheer, H.; Zinth, W.; Wachtveitl, J. *Chem. Phys.* **1995**, *197*, 297.

(15) Schmidt, S.; Arlt, T.; Hamm, P.; Lauterwasser, C.; Finkele, U.; Drews, G.; Zinth, W. *Biochim. Biophys. Acta* **1993**, *1144*, 385.

(16) Wachtveitl, J.; Huber, H.; Feick, R.; Rautter, J.; Müh, F.; Lubitz, W. *Spectrochim. Acta A* **1998**, *54*, 1231.

(17) Finkele, U.; Dressler, K.; Lauterwasser, C.; Zinth, W. In *Reaction Centers of Photosynthetic Bacteria*; Michel-Beyerle M.-E., Ed.; Springer-Verlag: Berlin, 1990; p 127.

(18) Schmidt, S.; Arlt, T.; Hamm, P.; Huber, H.; Nägele, T.; Wachtveitl, J.; Zinth, W.; Meyer, M.; Scheer, H. *Spectrochim. Acta A* **1995**, *51*, 1565.

(19) Rosker, M. J.; Wise, F. W.; Tang, C. L. *Phys. Rev. Lett*. **1986**, *57*, 321.

(20) Fragnito, H. L.; Bigot, J.-Y.; Becker, P. C.; Shank C. V. *Chem. Phys. Lett.* **1989**, *160*, 101.

(21) Mokhtari, A.; Chebira, A.; Chesnoy, J. *J. Opt. Soc. Am. B* **1990**, *7*, 1551.

(22) Wang, Q.; Schoenlein, R. W.; Peteanu, L. A.; Mathies, R. A.; Shank, C. V. *Science* **1994**, *266*, 422.

(23) Zinth, W.; Huppmann, P.; Arlt, T.; Wachtveitl, J. *Philos. Trans. R. Soc. London A* **1998**, *356*, 465.